aerospace

MDPI

Article

Optimization of Pyroshock Test Conditions for Aerospace Components to Enhance Repeatability by Genetic Algorithms

Wonki Bae [1,2] and Junhong Park [2,*]

[1] Korea Testing Laboratory, 10, Chungui-ro, Jinju-si 52852, Gyeongsangnam-do, Republic of Korea; wkbae@ktl.re.kr
[2] Department of Mechanical Engineering, Hanyang University, 222, Wangsimni-ro, Seongdong-gu, Seoul 04763, Republic of Korea
* Correspondence: parkj@hanyang.ac.kr

Abstract: Electronic components assembled in satellites should be able to withstand the vibration, noise, and impact loads generated by space vehicles during launch. To simulate the impact loading in a laboratory environment, a pyroshock test simulates an impact load resulting from explosions during the stage and pairing separation of launch vehicles, which imposes significant stress on the components, potentially leading to failures and damage. To ensure component reliability before the flight model (FM) stage, where components are mounted on the actual launch vehicle and sent into orbit, a pyroshock test is conducted during the qualification model (QM) stage using identical parts and specifications. This process involves measurements of the acceleration induced by pyroshock to calculate the shock response spectrum (SRS) and evaluate the components' reliability against the required SRS to confirm their ability to endure the shock and operate normally in post-tests. The aerospace developer determines the SRS requirements based on the space launch vehicle and the installation location of the electronic components. Configuring a suitable pyroshock test to meet these requirements typically involves extensive trial and error. This study aims to minimize such trial and error by examination of SRS changes through a numerical approach by table structural vibration analysis. The structure is subjected to in-plane impacts using a steel ball via a pendulum method. Various SRS profiles are calculated by test factors such as the weight of the steel ball, the pendulum angle, and the installation position of the test specimen. Furthermore, a genetic algorithm is utilized to derive the optimal test conditions that satisfy the required SRS. An automated pyroshock test system is developed to enhance repeatability and reduce human errors.

Keywords: pyroshock testing; shock response spectrum; longitudinal vibration; genetic algorithm; optimization; repeatability

check for updates

Citation: Bae, W.; Park, J. Optimization of Pyroshock Test Conditions for Aerospace Components to Enhance Repeatability by Genetic Algorithms. *Aerospace* **2024**, *11*, 700. https://doi.org/10.3390/aerospace11090700

Academic Editor: Hyun-Ung Oh

Received: 19 July 2024
Revised: 19 August 2024
Accepted: 20 August 2024
Published: 26 August 2024

Copyright: © 2024 by the authors. Licensee MDPI, Basel, Switzerland. This article is an open access article distributed under the terms and conditions of the Creative Commons Attribution (CC BY) license (https://creativecommons.org/licenses/by/4.0/).

1. Introduction

In the aerospace and defense industries, pyroshock tests are crucial to ensuring the structural integrity of electronic and optical components. When pyrotechnic explosives detonate during separation events, antenna activations, or solar panel deployments, they generate intense shock waves known as pyroshocks. These shocks differ significantly from ordinary vibration events. While large components and structures with lower resonance frequencies often sustain minimal damage due to the short wavelength of pyroshocks, sensitive electronic and optical components can be seriously affected. Such damage poses a significant risk to the success of missions.

The objectives of pyroshock tests are outlined in multiple standards, which include procedures for evaluation of the durability and reliability of components that have to endure external shocks. These standards ensure consistency in testing through standardized techniques [1–5]. The impact forces range from 1000 to 10,000 g, classified as near-field, mid-field, and far-field shocks. Each shock type requires specific testing techniques, protocols, and apparatus to accurately reproduce these forces in a consistent manner [6–13].

The Shock Response Spectrum (SRS) is crucial for the analysis of shock environments in aerospace components. SRS offers a frequency-based depiction of a shock's impact on structures, enabling engineers to predict how different spacecraft components will respond to such shocks. This insight is crucial for designing more resilient systems and devising effective mitigation strategies. Various experimental and numerical methods have been developed to accurately predict pyroshock responses in spacecraft structures. Ding [14] introduced a new methodology, validated through light-gas gun tests using a virtual mode synthesis method and an acceleration frequency response function. Choi [15] proposed an innovative experimental technique that combined in-line filtering with laser pulse stimulation, achieving high accuracy and cost-effectiveness in predicting pyroshock responses. Wang et al. [16] explored the application of stress wave theory to model and predict pyroshock responses at the spacecraft-rocket interface, providing valuable insights into mitigation strategies. Yalçinkaya and Gürsoy [17] compared experimental results from metal-to-metal impact tests with finite element (FE) simulations. The comparison demonstrated high agreement for the study of the numerical validation of pyroshock test systems using explicit FE simulations.

Moreover, the study by Gour et al. on the tear and fracture of elastomeric skins in morphing wings underscores the broader relevance of stress and shock management in aerospace applications. Their research on mechanical stresses, including tear and fracture in morphing wings, parallels the challenges encountered in pyroshock testing, where accurate testing and modeling are crucial for ensuring the reliability and performance of aerospace components under extreme conditions [18].

This research aims to identify optimal test conditions that meet specific requirements while minimizing the stress on test specimens caused by repeated incorrect test executions. Conventional test methods require extensive trial and error to find conditions that satisfy the requirements, leading to significant time and resource losses. To minimize this trial and error, this study investigates the changes in the shock response spectrum (SRS) using a numerical approach to structural vibration analysis and employs a genetic algorithm to quickly and accurately determine the optimal test conditions. In a pendulum-based testing apparatus, the weights of the steel ball, the angles of the pendulum, and the installation positions of the test specimen on the table structure result in approximately 2000 possible combinations. The genetic algorithm quickly and accurately identifies the optimal test conditions. An automated pyroshock test system is designed to enhance repeatability and reduce human errors, ensuring precise test execution.

2. Experimental Study of the Pyroshock Tests

2.1. Quantification of Vibration Damage

The SRS is a crucial tool in estimation of vibration damage for analyzing and quantifying shock environments. It describes the relationship between the maximum response and the natural frequency of a series of single-degree-of-freedom (SDOF) oscillators subjected to a given table structure excitation. The SRS transforms time-domain shock excitations into a frequency-domain representation. The transformed magnitude is expressed in terms of displacement, velocity, or acceleration. This method is particularly valuable in the aerospace, electronics, and mechanics industries for specifying shock test parameters and design for environmental adaptability.

The SRS was introduced by Biot in the 1930s during his studies on the impact of earthquakes on buildings. By the 1940s, SRS plots were being generated using analog computers, significantly reducing the complexity and volume of data required to describe a shock event [7,19,20]. The SRS represents a transient shock acceleration response in the frequency domain, defined as the relationship between the peak absolute magnitude and the natural frequency of a series of SDOF oscillators, each with different frequencies but subjected to the same shock transient load. The calculation process involves conversion of a time-domain impulse excitation into the SRS representation in the frequency domain [9].

To calculate the SRS, the time-domain shock response is transformed into the frequency-domain representation to understand how different frequency components of a shock impact a system. The process begins with an acceleration input, typically an acceleration-time history of the shock event. A series of SDOF systems, each with a different natural frequency but the same damping ratio, is used to analyze the response. The response of each SDOF system to the input acceleration is computed using numerical methods such as the Newmark-beta method, Runge–Kutta, or digital filters. The peak response of each system is then plotted against the natural frequency to form the SRS. The ramp-invariant method is commonly employed for its computational efficiency and accuracy. This method approximates the continuous transfer function with a discrete transfer function using digital filters, allowing the calculation of the acceleration response in the time domain. The resulting SRS curve provides a comprehensive view of the maximum responses across various frequencies, which is crucial for the design of systems capable of withstanding shock environments [21].

A typical SRS graph is shown in Figure 1, and several factors affect the SRS. The duration of the shock has the most significant impact on the shape and trend of the SRS, especially at low frequencies. Longer durations result in higher amplitudes due to the greater energy transferred to the system. While the amplitude of the shock affects the overall amplitude of the SRS, it does not change its trend; the SRS amplitude is proportional to the shock input signal amplitude. Different waveforms can influence the frequency point of peak acceleration but have a minor effect on the overall envelope of the SRS [7,19].

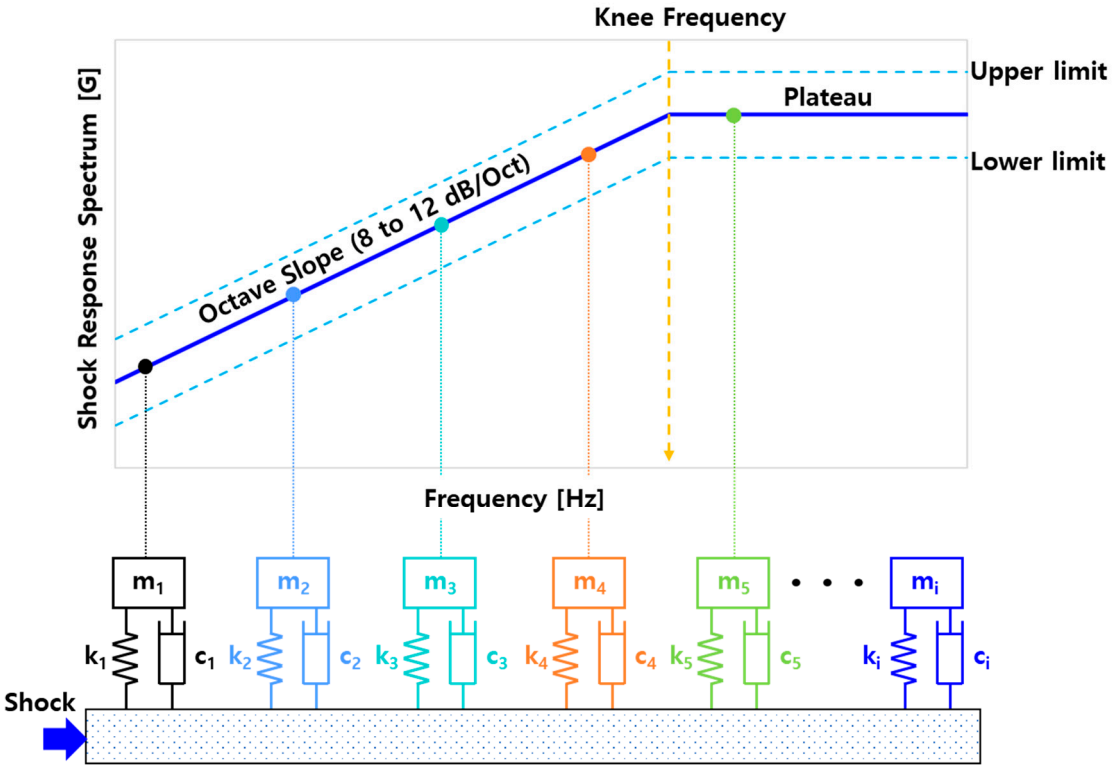

Figure 1. SRS predictions in the frequency domain.

2.2. Pyroshock Test Standard

The pyroshock testing standards which are most often referred to are summarized in Tables 1 and 2 [1–4]. Impact forces are grouped by intensity into three categories, namely near-field, mid-field, and far-field. Each category requires unique testing methods, processes, and equipment to correctly reproduce the corresponding impact forces.

Table 1. Summary of pyroshock test standards.

Standard	Title	Purpose	Features
NASA-STD-7003A	Pyroshock Test Criteria	To establish guidelines for simulating and measuring the impact of pyroshocks on aerospace vehicles	- Establishes pyroshock levels for equipment and components used in space missions - Provides detailed instructions for the measurement, evaluation, and testing of pyroshock
ECSS-E-ST-10-03C	Space Engineering–Testing	To describe testing procedures and principles for evaluating space hardware and systems	- Delivers an extensive overview of the environmental testing required for space missions - Presents a broad approach to multiple environmental tests, including pyroshock
MIL-STD-810H	Environmental Engineering Considerations and Laboratory Tests	To outline test methods and procedures for replicating environmental conditions affecting military equipment	- Provides test methods for a broad spectrum of environmental conditions - Includes pyroshock as one of the environmental tests covered
MIL-STD-1540D	Test Requirements for Space Vehicles	To establish test requirements for space vehicles	- Provides detailed guidelines on test requirements for space vehicles and their subsystems - Encompasses pyroshock testing procedures, criteria, and methods for data analysis

Table 2. Classification of Pyroshock.

Standard	Intensity	Max. Acceleration (g)	Max. Frequency (kHz)	Test Method
MIL-STD-810H	Near-field	10,000 or more	10 or more	- Explosives explosion
	Mid-field	10,000 or less	3~10	- Mechanical test devices
	Far-field	1000 or less	3 or less	- Mechanical test devices - Electric exciters
NASA-STD-7003A	Near-field	5000 or more	100 or more	- Explosives explosion
	Mid-field	1000~5000	10 or more	- Mechanical test devices
	Far-field	1000 or less	10 or less	- Mechanical test devices - Electric exciters

This research details the execution of a pyroshock test using a pendulum-based mechanical device. In this system, a steel ball mounted on a pendulum arm impacts a structure to generate pyroshock loads. The electronic components are installed on the structure to assess their response to the shock. The kinetic energy transferred from the pendulum to the structure creates the pyroshock loads. The shock energy level can be adjusted by varying the weight of the steel ball and the angle of the pendulum. Similar procedures are applicable to the other test methods.

2.3. Various Pyroshock Test Equipments

Many testing procedures conduct pyroshock tests using various impact sources. The test equipment used by each procedure is classified according to its specific testing methods.

2.3.1. Pendulum Method

The pendulum method is one of the most commonly used techniques among pyroshock test methods. To implement test conditions that meet specific requirements, various combinations of hammer weights, shapes, and boundary conditions are employed. While the shapes of the pendulums may vary, they share a common principle of controlling the hammer's potential energy by adjusting the length and angle of the pendulum. To prevent multiple impacts due to rebound, the string connected to the pendulum is held securely [22–29].

2.3.2. Pneumatic Projectile Method

In this configuration, the movement of the hammer along the guide is regulated by pressurized air, analogous to the trajectory of a bullet through a gun barrel. To meet the specified requirements, various parameters are adjusted, including the thickness of the resonant plate, the boundary conditions, and the impact load. The impact load is controlled by the type of hammer and the air pressure. This method ensures that multiple impacts due to rebound do not occur [30–46].

2.3.3. Nail Gun Method

The nail gun method represents a cost-effective and practical approach for performing the pyroshock tests. By utilizing the kinetic energy of commercial nail guns, this method eliminates the need to manufacture separate equipment such as pendulum or pneumatic hammer guides. Compared with the previously mentioned methods, the nail gun approach also offers excellent repeatability [47–50].

2.4. Experimental Setup to Implement Pyroshock

This study performs a pyroshock test based on the pendulum method, as illustrated in Figure 2a. To conduct the pyroshock test, a pendulum weight ranging from 12 to 30 kg is used to impact a rectangular table structure. The pendulum angle can be adjusted from 10 to 90 degrees. The test operator uses a protractor to visually set the pendulum angle, aiming to establish a test arrangement that meets the specifications. However, due to the reliance on the operator's visual estimate, the applied load varies depending on the operator. The operator holds an additional string, which is released to deliver the impact. To prevent secondary impacts, the string is recaptured immediately after the initial impact. Determining the suitable test configuration is often a trial-and-error process that can take one to two days. The accelerometer (352B70, PCB Piezotronics, New York, NY, USA) is used for the longitudinal vibration measurements. The measured accelerations are digitized using the Simcenter SCADAS Mobile 05 module (SIEMENS, Munich, Germany) and subsequently stored and analyzed with Simcenter Testlab (Version 18).

2.5. Application of Genetic Algorithm (GA) for Test Parameter Optimizations

The GA is a class of optimization algorithms inspired by the principles of natural selection and genetics. Introduced in 1975, GAs belong to the broader family of evolutionary algorithms (EAs), which include Evolutionary Programming (EP), Evolution Strategies (ES), and Genetic Programming (GP). The key components of GAs include a population of potential solutions (chromosomes), a fitness function to evaluate the suitability of these solutions, and genetic operators such as selection, crossover, and mutation that guide the evolution of the population towards optimal solutions. The process begins with the initialization of a random population, followed by iterative cycles of evaluation, selection, reproduction, and replacement until a termination criterion is met [51].

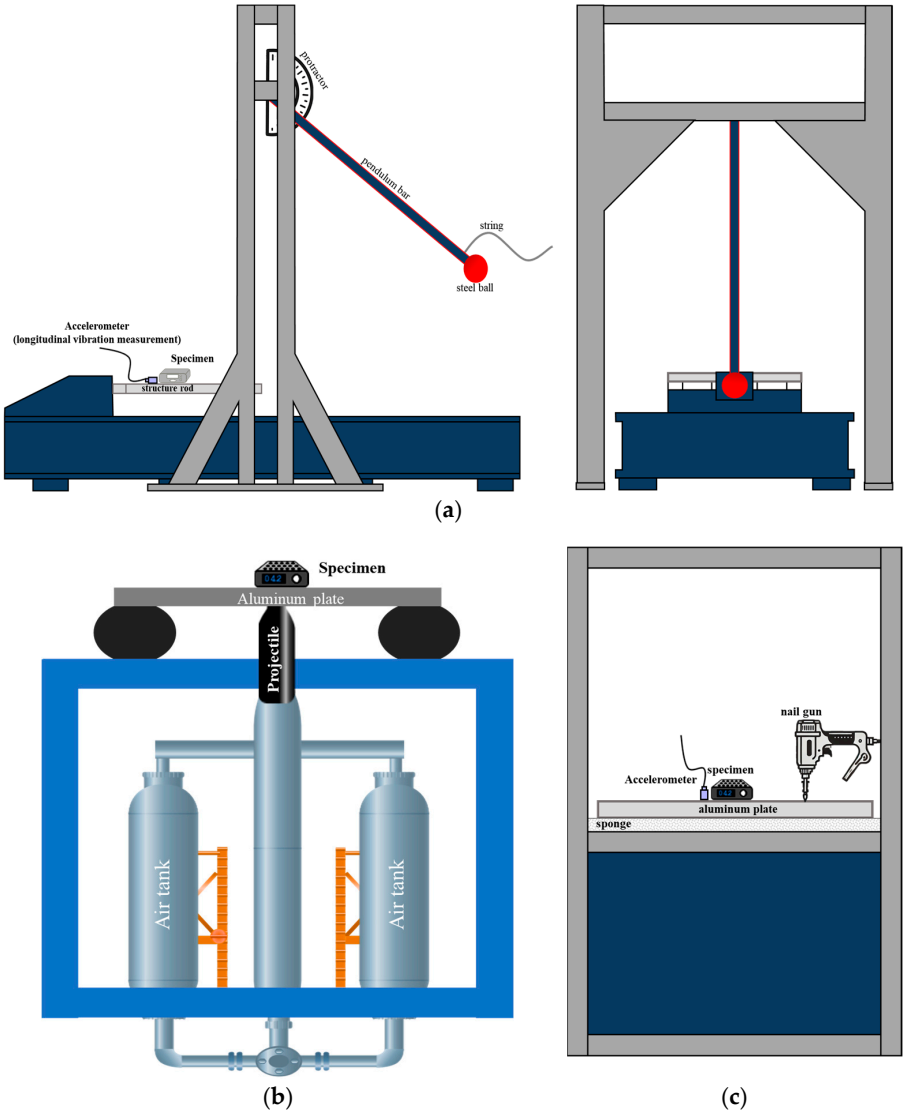

Figure 2. Various pyroshock test methods. (**a**) Pendulum method; (**b**) Pneumatic projectile method; (**c**) Nail gun method.

The main strength of GAs lies in their ability to perform global optimization in complex landscapes, making them highly suitable for problems where traditional methods, such as non-linear, multi-modal, or high-dimensional spaces, struggle. They are widely applied in fields of engineering design, machine learning, scheduling, and evolutionary robotics. GAs excel in finding global optima, avoiding the pitfalls of local optima that often trap gradient-based methods. Their robustness allows them to perform well even when the objective function is noisy or discontinuous, and their flexibility enables them to handle various types of variables and constraints effectively [52].

The GA is a well-established optimization technique widely used across various applications. Sun et al. [53] introduced an adaptive genetic algorithm (AGA) to optimize the synthesis of pyroshock acceleration profiles. The AGA dynamically adjusted its parameters to enhance convergence and performance, aiming to minimize the error between the synthesized and target shock response spectrum (SRS). This adaptive mechanism significantly improved the algorithm's accuracy and computational efficiency by avoiding local optima and identifying a global solution. Viale et al. [54] applied a GA to optimize the shape and size of a resonant plate for pyroshock testing. The GA determined geometric parameters and utilized a CAD modeler and finite element (FE) solver to predict the plate's behavior. By adjusting parameters to minimize the SRS error, the GA ensured that the plate

met shock test requirements while avoiding local minima. Additionally, Viale et al. [55] used a GA to optimize parameters of a pyroshock test simulation model, iterating through a population of potential solutions and applying genetic operators to minimize discrepancies between simulated and experimental SRS. This iterative process evolved solutions toward the optimal parameter set, enhancing the simulation model's accuracy. Monti et al. [56] employed a GA in a two-level optimization strategy to determine optimal parameters for simulating dynamic loads in space structures. The GA conducted a global search to identify a satisfactory parameter set, which was further refined using a heuristic algorithm. This approach helped avoid local optima and iteratively improved parameters through selection, crossover, and mutation operations. Chen et al. [57] investigated optimized actuator positions for active vibration control in a GARTEUR aircraft model. He employed a genetic algorithm, integrating controllability, observability criteria, and system energy criteria. The method involved encoded actuator positions as chromosomes and using selection, crossover, and mutation to identify positions that greatly improved vibration control performance.

As illustrated in Figure 3, this paper presents a study that utilized GA to iteratively optimize the combination of the weight mass, the pendulum angle, and the specimen location. The objective was to identify conditions that satisfy SRS requirements in the formulation of longitudinal vibration. The control variables, objective function, constraints, and parameters used in the genetic algorithm are summarized in Table 3. Four types of mass were considered: 12, 18, 24, and 30 kg. The angle varied from 10 to 90 degrees, resulting in 81 discrete values. The specimen position on the pyroshock test equipment ranged from 0.2 to 0.7 m in six increments. Consequently, 2 bits were used for the mass, 7 bits for the angle, and 3 bits for the position, resulting in a total of 12 bits per chromosome to represent these values in the GA. For example, encoding a mass of 18 kg, an angle of 45 degrees, and a position of 0.5 m yielded [01] for the mass, [0101101] for the angle, and [011] for the position. Thus, the chromosome was represented as [010101101011].

Table 3. Genetic algorithm optimization parameters.

Aspect	Details
Control Variables	- Mass (m1): Discrete values, {12, 18, 24, 30} kg - Angle (θ): Range from 10° to 90° - Position (x): Discrete positions: {0.2~0.7} m
Objective Function	Minimize the sum of squared differences between the calculated SRS and the required SRS, plus penalties for violating upper and lower SRS limits $\text{Cost} = \Sigma(\max(0, \lvert SRS_{calc,i} - SRS_{req,i} \rvert))^2 + \lambda \cdot \Sigma(\max(0, SRS_{calc,i} - SRS_{upper,i}) + \max(0, SRS_{lower,i} - SRS_{calc,i}))$ where - SRScalc,i: the calculated SRS - SRSreq,i: the required SRS - SRSlower,i, SRSupper,i: lower and upper allowable SRS limits - λ: a weighting factor
Constraints	- Mass constraint: m ∈ {12, 18, 24, 30} - Angle constraint: $10° \leq \theta \leq 90°$ - Position constraint: x ∈ {0.2~0.7} - SRS values must not exceed the defined upper limit or fall below the defined lower limit
GA Parameters	- Population size, Max generations - Crossover fraction, Mutation - Gaussian with a rate of 0.01 - Selection: Tournament selection - Elitism: Top 10 individuals preserved from each generation

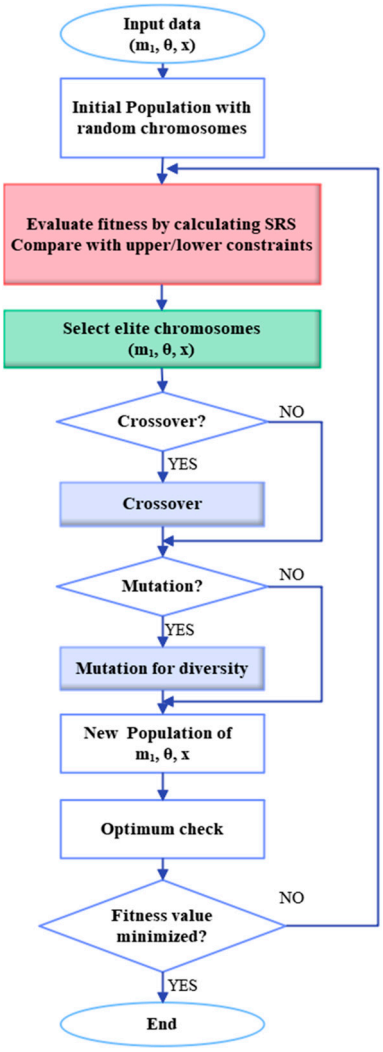

Figure 3. Flow chart of the genetic algorithm used for shock test parameters.

3. Prediction of Impacted Wave Propagation

3.1. Modeling of Structure Vibration Undergoing Pyroshocks

The pendulum method is used in this study to investigate the dynamics of an aluminum rectangular structure impacted by a steel ball. The system, shown in Figure 4, consists of an aluminum structure with length L and mass M, and a pendulum with length l and mass m_1, inclined at an angle θ. The pendulum impacts the structure, resulting in dynamic behavior. When the structure is subjected to a longitudinal impact, the resulting excitation primarily induces longitudinal vibrations. Since transverse modes receive negligible energy input from such an impact, they contribute minimally to the overall vibrational response. Also, most SRS requirements specify a knee frequency in the range of 1000 to 3000 Hz. The first natural frequency of transverse vibrations that directly influences the knee frequency is approximately 200 Hz and can therefore be considered negligible. Consequently, the transverse vibration components were excluded from this analysis.

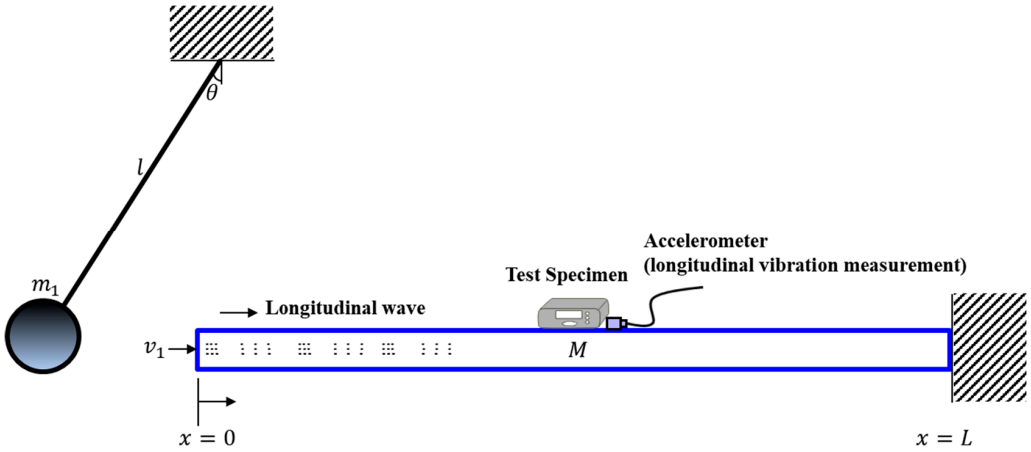

Figure 4. Analytical model of pyroshock test system using longitudinal wave propagation.

3.2. Governing Equation of the Structure Vibration

The longitudinal vibration of the structure induced by the pendulum's impact was expressed as

$$\frac{\partial^2 u}{\partial x^2} = \frac{1}{c^2}\frac{\partial^2 u}{\partial t^2} \tag{1}$$

$$u(x,t) = \sum_{n=1}^{\infty}\left[(Asin\frac{\omega_n}{c}x + Bcos\frac{\omega_n}{c}x)(Dsin\omega_n t + Ecos\omega_n t)\right] \tag{2}$$

Applying the boundary conditions of a fixed-free table structure, $u_{x=0} = 0$ and $\left(\frac{\partial u}{\partial x}\right)_{x=L} = 0$

$$u(x,t) = \sum_{n=1,3,5,\ldots}^{\infty}\left[(Asin\frac{n\pi}{2L}x)(Dsin\frac{n\pi}{2L}ct + Ecos\frac{n\pi}{2L}ct)\right] \tag{3}$$

$$\omega_n = \frac{n\pi}{2L}c, (n = 1,3,5\cdots) \tag{4}$$

By simplifying the coefficients, the above vibration response was rewritten as follows.

$$u(x,t) = \sum_{n=1,3,5,\ldots}^{\infty}\left[(sin\frac{n\pi}{2L}x)(D_n{\cdot}sin\frac{n\pi}{2L}ct + E_n{\cdot}cos\frac{n\pi}{2L}ct)\right] \tag{5}$$

By applying the initial conditions $u(x,0) = 0$, $\dot{u}(x,0) = V'$, the displacement and acceleration are expressed as follows.

$$u(x,t) = \frac{8V'L}{\pi^2 c}\sum_{n=1,3,5,\ldots}^{\infty}\left[\frac{1}{n^2}{\cdot}sin\frac{n\pi}{2L}x{\cdot}sin\omega_n t\right] \tag{6}$$

$$\ddot{u}(x,t) = -\frac{8V'L}{\pi^2 c}\sum_{n=1,3,5,\ldots}^{\infty}\left[\frac{\omega_n^2}{n^2}{\cdot}sin\frac{n\pi}{2L}x{\cdot}sin\omega_n t\right] \tag{7}$$

The interaction between the steel ball and the beam before and after the shock is explained by the Hertzian contact theory and is shown in Figure 5. It can be written as the Equation (8).

$$F = k\delta^{3/2} \tag{8}$$

where $k = \frac{4}{3}E_*\sqrt{R}$ and $E_* = \frac{E_1E_2}{E_1(1-\nu_2^2)+E_2(1-\nu_1^2)}$.

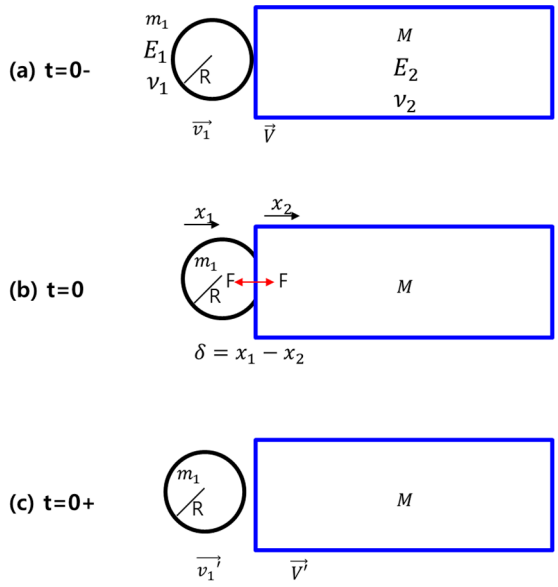

Figure 5. Hertzian contact model when hitting the structure.

The following established relationship $\ddot{x}_1 = \frac{F_1}{m_1}$, $\ddot{x}_2 = \frac{F_2}{M}$ and $F_1 = -F_2 \equiv F$ is used to simplify the equation. The relative acceleration between the steel ball and the structure can be described as $\ddot{\delta} = \ddot{x}_1 - \ddot{x}_2 = -\left(\frac{1}{m_1} + \frac{1}{M}\right)F = -\frac{m_1+M}{m_1 M}F$. Utilizing Equation (8), the above equation is rewritten as $\dot{\delta}d\dot{\delta} = -\frac{m_1+M}{m_1 M}k\delta^{\frac{3}{2}}d\delta$. Applying the initial condition at $t = 0-$, where $\delta = 0$ and $\dot{\delta} = v_1 - V = v_1$, and performing integration, we get:

$$\frac{1}{2}\left(\dot{\delta}^2 - v_1^2\right) = -\frac{m_1 + M}{m_1 M}\frac{2}{5}k\delta^{\frac{5}{2}} \tag{9}$$

Because the maximum relative displacement δ_{max} is obtained at $\dot{\delta} = 0$, δ_{max} and F_{max} are written as $\delta_{max} = \left(\frac{5}{4k}\frac{m_1 M}{m_1+M}v_1^2\right)^{\frac{2}{5}}$, $F_{max} = k\delta_{max}^{\frac{3}{2}}$. Applying the law of energy conservation,

$$\text{(a) t} = 0- : \ \frac{1}{2}m_1\vec{v_1}^2 + \frac{1}{2}M\vec{V}^2 \tag{10}$$

$$\text{(b) t} = 0 : \ \int_0^{\delta_{max}} F d\delta = \frac{2}{5}k\delta_{max}^{\frac{5}{2}} \tag{11}$$

$$\text{(c) t} = 0+ : \ \frac{1}{2}m_1\vec{v_1}'^2 + \frac{1}{2}M\vec{V}'^2 \tag{12}$$

the Equations (11) and (12) are equivalent.

$$\frac{2}{5}k\delta_{max}^{\frac{5}{2}} = \frac{1}{2}m_1\vec{v_1}'^2 + \frac{1}{2}M\vec{V}'^2 \tag{13}$$

Also, by Impulse-momentum principle, $m_1\vec{v_1} + M\vec{V} = m_1\vec{v_1}' + M\vec{V}'$ and it is written as

$$\vec{v_1}' = \frac{1}{m_1}\left(m_1\vec{v_1} - M\vec{V}'\right) \tag{14}$$

By substituting Equation (14) into Equation (13) and simplifying the expression, the following result is obtained.

$$\frac{m_1 M + M^2}{2m_1}\vec{V}'^2 - M\vec{v_1}\vec{V}' + \frac{1}{2}\left(1 - \frac{M}{m_1 + M}\right)m_1\vec{v_1}^2 = 0 \tag{15}$$

$$\vec{V'} = \frac{m_1 \vec{v_1}\left(M \pm \sqrt{2M^2 - M_*}\right)}{M_*} \tag{16}$$

where $M_* = m_1 M + M^2$.

Here, $\vec{v_1}$ was derived from the relationship between the pendulum length and the angle. The longitudinal vibration of the table structure is formulated as follows:

$$\ddot{u}(x,t) = -\frac{8L}{\pi^2 c}\frac{m_1\sqrt{2gl(1-cos\theta_{max})}(M \pm \sqrt{2M^2 - M_*})}{M_*}\sum_{n=1,3,5,\ldots}^{\infty}\left[\frac{\omega_n^2}{n^2}\cdot sin\frac{n\pi}{2L}x\cdot sin\omega_n t\right] \tag{17}$$

4. Improvement of Test Repeatability

4.1. Overview of the Test

MIL-STD-7003A and ECSS-E-ST-10-03C provide detailed descriptions of the procedures and requirements for the pyroshock tests. These standards specifically address the shock level and tolerance of the SRS and stipulate that the shock duration in the time domain should not exceed 20 ms. In the pendulum-based pyroshock test equipment discussed in this paper, the conditions such as impact energy and impact time are determined by the angle of the pendulum and the mass of the weight. As illustrated in Figure 6, an increase in the angle and mass of the weight leads to a corresponding increase in transient acceleration responses, resulting in a higher amplitude in the SRS. The increased vibration amplitude affects the impact duration. By precisely controlling the impact parameters, it is possible to achieve the desired SRS with improved repeatability.

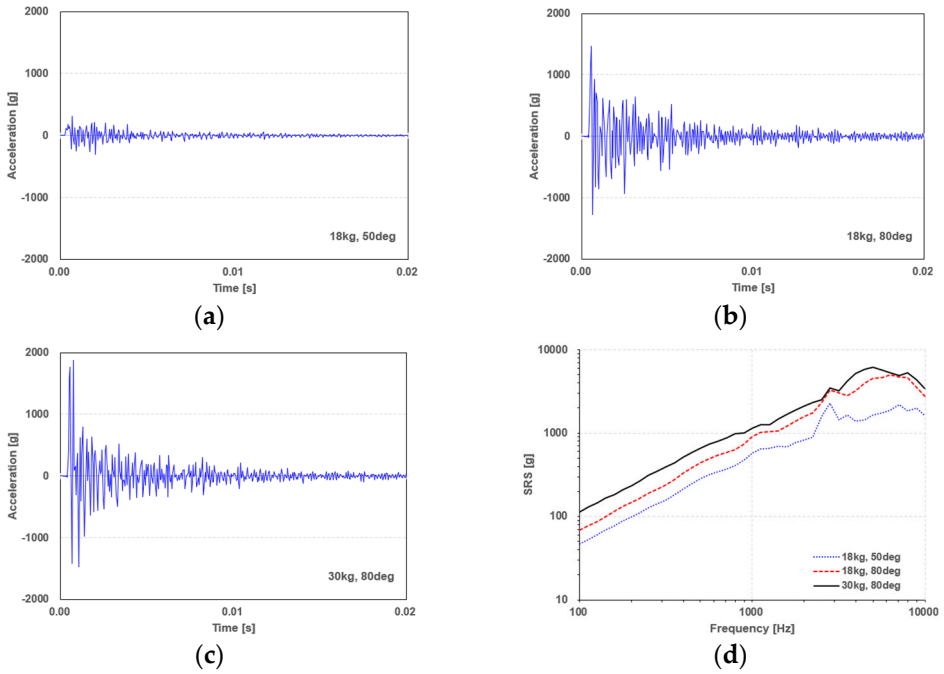

Figure 6. Comparison of transient acceleration response and SRS with the varying mass and angle. Vibration responses for (**a**) mass 18 kg, angle 50°, (**b**) mass 18 kg, angle 80°, and (**c**) mass 30 kg, angle 80°. (**d**) The resulting SRS obtained with different test conditions.

4.2. The Need to Improve Test Repeatability

In this test, the precise motion of the pendulum is crucial. However, manually initiating the pendulum's motion leads to discrepancies in release timing and method, reducing the reliability and repeatability of the measured data. Use of a release aid device, similar to those used in archery, enhances the consistency of the tests.

To maintain consistent pendulum motion, all experimental conditions should be identical for each trial. Manual release introduces various issues, including timing variability, procedural inconsistency, and human error. Archery release aids prevent micro-movements

of the fingers, ensuring a uniform release of the bowstring. Application of this concept to the pendulum improves the repeatability of the experiments involving a pendulum and steel ball.

Several studies have demonstrated the efficacy of automated release mechanisms in pendulum tests. Brüggemann et al. [58] described the development of an automated modal pendulum for experimental modal analysis that provides consistent force application and reduces errors compared with manual methods. This automated method enhances data quality and reliability, making it a valuable tool for assessing the dynamic behavior of milling machines. According to Wikipedia, a release aid in archery allows archers to achieve more consistent and accurate releases by mechanically releasing the bowstring, thereby eliminating human error and finger strain. By emulating this approach, an automated pyroshock equipment was designed, significantly enhancing the reproducibility and repeatability of pendulum-based tests, resulting in more accurate and consistent test outcomes.

4.3. Design of an Automated Testing Device

An automated testing device was developed to address the issues associated with manual pendulum release. This system consistently positioned the steel ball at a predetermined height and discharged it evenly. Precision motors and reducers controlled the motion of the pendulum and ensured precise drop placements. To prevent re-impact from rebound after the initial impact, a stopper device was included. This system ensured the accuracy and repeatability of the tests by preventing multiple impacts due to rebound.

The automated testing equipment improved three critical factors: the uniform timing of the pendulum's release, the accurate alignment of the pendulum's initial position, and the prevention of re-impact. By maintaining consistent release conditions and minimizing multiple impacts, the automated test system effectively compensated for the drawbacks of manual tests.

4.4. Application to the Test Specimen

The developed automated test equipment was used to conduct pyroshock tests on the circuit board. A circuit board is an essential tool for verifying the accuracy and quality of electronic circuit designs and assembly processes, particularly for space applications. This board includes various surface mount technology components, such as a ball grid array and a quad flat package. According to the SRS requirements, electronic components are more significantly affected by high-frequency shocks than low-frequency ones, leading to critical issues from an electrical perspective rather than structural damage. To assess the integrity of the test specimens, visual inspections and simple electrical characteristic tests were performed before and after the pyroshock tests.

5. Results and Discussion

5.1. Comparison of Results between Analysis and Experiment

The estimated accelerations in a fixed-free beam impacted by a steel ball were compared with measured responses. The SRS was calculated using a Tom Irvine algorithm [6]. The following procedures were used to determine the test settings. Conditions that satisfied the requirements were identified using analytical data. These conditions were applied during the test. After the test, the results were compared with the analytical predictions and assessed for compliance with the requirements. Figure 7 confirms the comparability and fulfillment of these conditions.

The experiments utilized a 24 kg steel ball with the pendulum set at a 50-degree angle. The results under these constant conditions were compared, revealing similar patterns across all frequency regions, with each result meeting the necessary requirements. This consistency indicated that the operating conditions could be efficiently anticipated using the analytical model, thereby reducing trial and error.

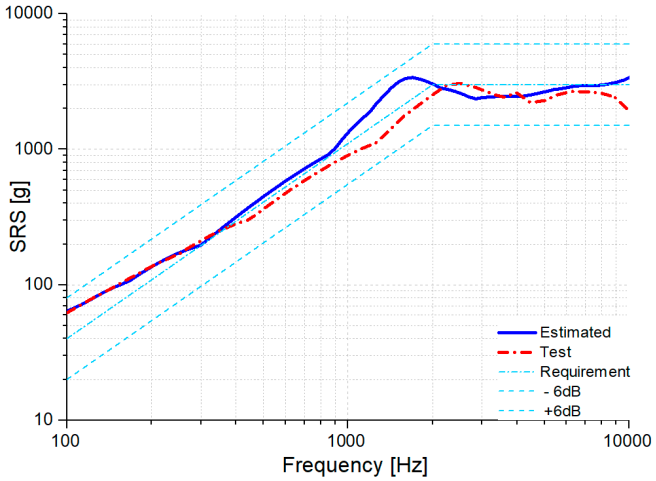

Figure 7. Comparisons of measured and predicted vibration responses.

The pendulum angle was adjusted within a range of 10 to 90 degrees, and the resulting SRS was displayed on a three-dimensional graph shown in Figure 8. As expected, SRS levels increased with rising pendulum angles. Furthermore, by overlaying the requirements and upper/lower limits onto the three-dimensional graph, a direct comparison was made to determine conformity with the requirements. The SRS exhibits an increasing trend with the increase in the mass of the weight. By adjusting the combination of angle and mass, it is possible to determine a test condition that satisfies the requirements.

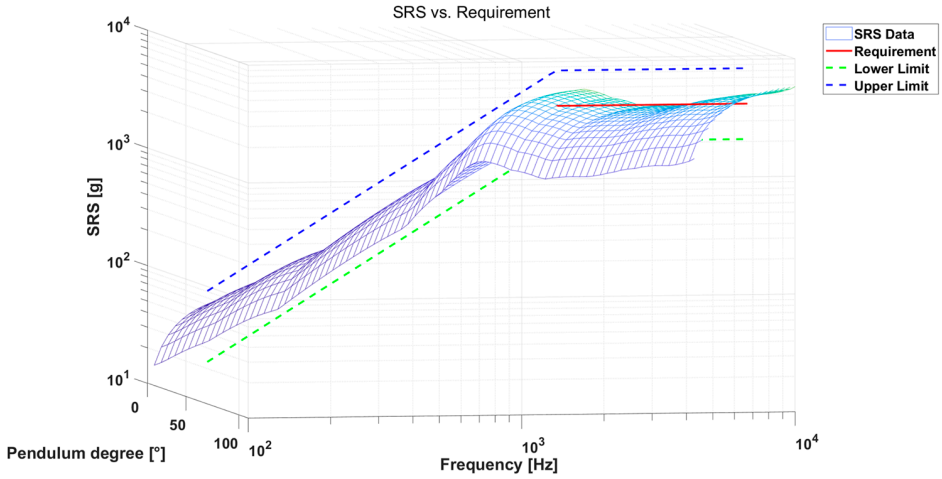

Figure 8. Effects of the pendulum angle and frequency on the estimated SRS.

5.2. Optimal Test Parameter Combinations via GA

The flowchart illustrating the process of obtaining the optimal combination of the mass (m_1) of the weight, the angle (θ) of the pendulum, and the location (x) of the specimen through a Genetic Algorithm is shown in Figure 3. The process begins with an arbitrary initial population, where the specified chromosome encoding for m_1, θ, and x is substituted into Equation (17) for the longitudinal vibration of the table structure to calculate vibration response and the SRS. These calculated SRS values are then compared with the requirements and constraints of the objective function. The elite chromosomes are retained, while the non-elite ones undergo mutation and crossover to generate a new population.

The objective function calculates the difference between the computed SRS results and the requirements, using the sum of the squares of these differences to determine the cost. Additionally, a penalty is applied if the computed SRS results exceed the upper or lower constraints. The fitness value is then calculated as the sum of the cost and penalty, with more weight potentially added to more critical factors. In this study, however, both cost and

penalty are considered equally significant and are weighted equally. The goal of the GA is to minimize the fitness value, thereby determining the optimal values for m_1, θ, and x. The GA parameters used for the optimization process in this paper are listed in Table 4.

Table 4. GA parameters for optimization process.

Algorithm Type	Population Size	Generation Size	Elite Count	Crossover Fraction	Mutation Function	Mutation Rate	Selection Function
Continuous	200	200	10	70%	Gaussian	20%	Tournament

Enhancing optimization capability and decision speed requires precise adjustment of genetic algorithm parameters tailored to the specific problem. This study considered four types of mass (m_1) at 12, 18, 24, and 30 kg, 81 angles (θ) ranging from 10 to 90 degrees, and six positions (x) ranging from 0.2 to 0.7 m on the pyroshock test equipment's pattern hole, resulting in a total of 1944 possible combinations ($4 \times 81 \times 6$). To select the appropriate parameters for this study, several examples were referenced, and a trial-and-error process was conducted. The GA parameters used are presented in Table 5. As illustrated in Figure 9, the SRS resulting from this parameter combination satisfies the specified requirements. Thee population size and generation size were set to 200, the elite count to 10, the crossover fraction to 70%, and the mutation rate to 20%. Although the generation size was set to 200, as shown in Figure 10, the best fitness value converged between 15 and 20 generations. Figure 11 illustrates how the combinations of a generation population vary throughout the optimization process.

Table 5. Optimal value of the parameters through GA.

Parameter	Value
Mass (m_1) [kg]	24
Angle (θ) [°]	29
Specimen location (x) [m]	0.6

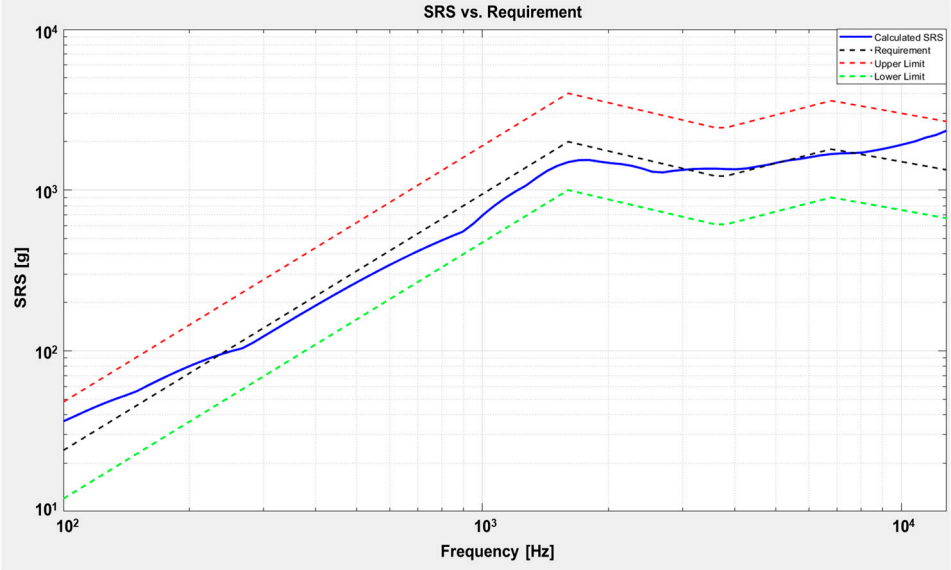

Figure 9. Comparison between the optimal SRS obtained through GA and the test requirements.

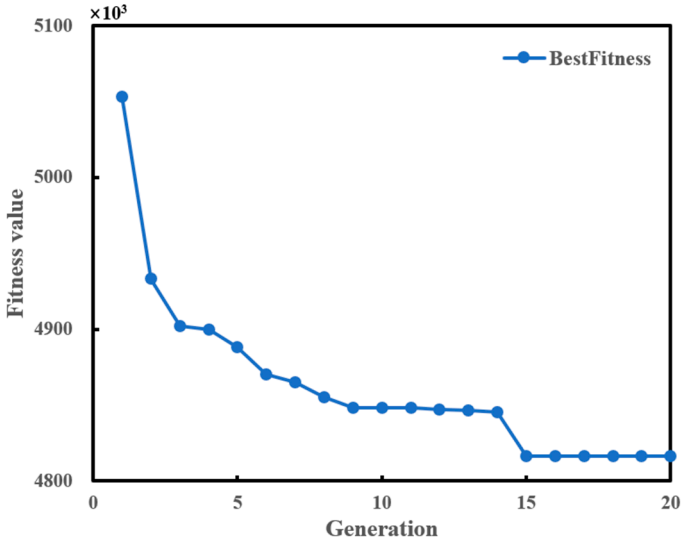

Figure 10. Convergence of objective functions to minimize the fitness value.

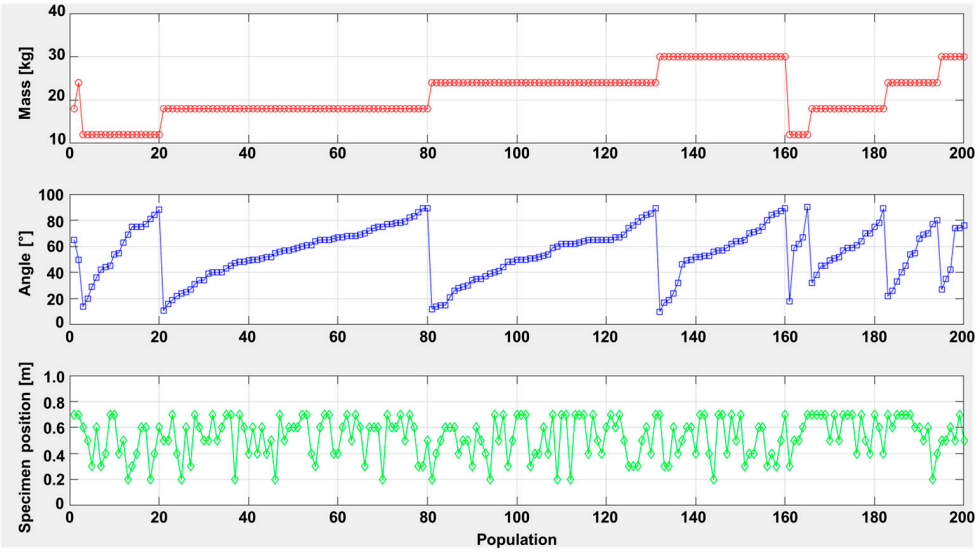

Figure 11. Combinations of a generation population.

5.3. Improvement of Repeatability through Automated Testing

The results of the automated and manual tests are compared in Figure 12. The solid line represents the results of ten repeated tests, while the light blue dotted line indicates the requirement, upper limit, and lower limit, respectively. The automated test results demonstrated consistent performance across all frequencies, whereas the manual test results showed limited repeatability, particularly at 4000 Hz. A box plot in Figure 13 clearly illustrates the variance between the two tests, highlighting the greater reliability of the automated method. To examine the repeatability variance between the automated and manual tests, four indicators were used: max/min ratio, coefficient of variation (CV), mean absolute deviation (MAD), and interquartile range (IQR). The results revealed comparable trends across all four indicators, with automated tests showing greater consistency across all frequencies.

Furthermore, the automated test resulted in considerable advantages in repeatability and productivity. The manual test required at least two people and took 238 s to complete, for a total of 476 person-seconds (TPS). In contrast, the automated system enabled one person to complete the identical test in 85 s. This resulted in a significant time-saving ratio, which represented an 82.14% improvement. In addition, the productivity increase rate

which measured how much productivity per person increased as a result of automation was calculated as 5.6. This substantial increase emphasized the significant improvement in workload capacity and employee efficiency achieved through the use of the automated testing methods. This not only accelerates the testing process, but also frees up human resources for other critical tasks, further enhancing overall operational efficiency.

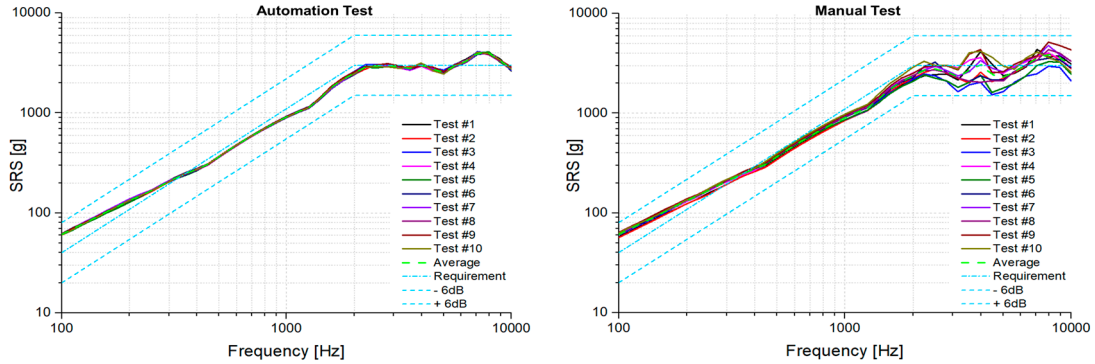

Figure 12. Test repeatability comparisons between automation and manual tests.

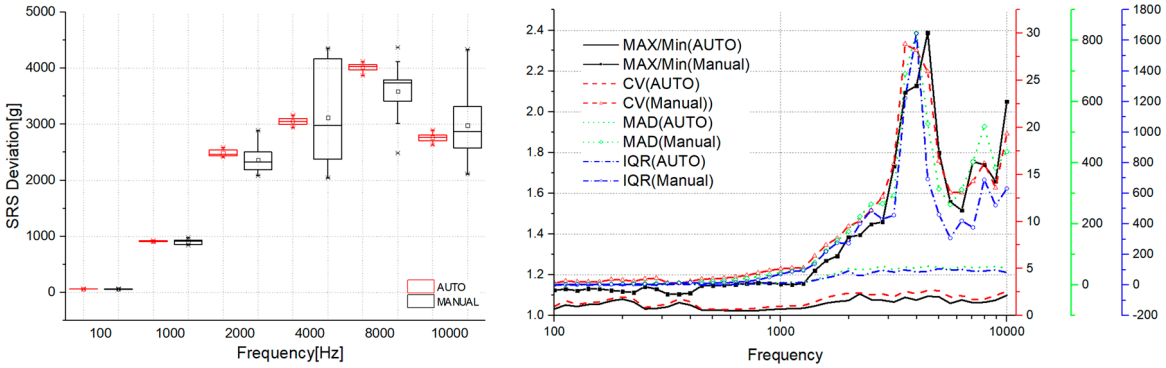

Figure 13. (**a**) Box plot and (**b**) four indicators comparison between automated and manual tests.

5.4. Determination of Abnormalities after the Pyroshock Test

The pyroshock test results for the circuit boards were subjected to comprehensive analysis. Circuit boards are essential tools for validating the accuracy and quality of the underlying circuit designs and assembly processes, especially in the context of space applications. These boards incorporate various surface mount technology (SMT) components, such as ball grid arrays (BGA), quad flat packages (QFP), and small outline integrated circuits (SOIC). These components play a critical role in evaluating soldering techniques, alignment precision, and electrical continuity, thereby ensuring the reliability and performance of the final electronic product. This validation process is vital for maintaining the high standards required for electronic components in space, where reliability is paramount.

It was observed that electrical devices are prone to resonant vibrations at high frequencies, which can potentially lead to failure. To investigate this, two identical circuit boards were subjected to pyroshock testing: one using automated pyroshock equipment and the other using a manual pyroshock test method. Visual inspections were conducted both before and after the pyroshock tests. Additionally, resistance measurements were taken at several pads on the circuit boards for comparison. The test conditions included a 24 kg weight, a pendulum inclination of 50 degrees, and the specimen mounted at a height of 0.6 m, with each sample being impacted ten times.

The results indicated that the test board (Sample #2) subjected to the automated pyroshock equipment showed no anomalies upon visual inspection and exhibited only minimal changes in resistance measurements. In contrast, the test board (Sample #1) sub-

jected to the manual pyroshock test method displayed no significant changes in resistance; however, it did exhibit detachment in a soldered section of the QFP. This detachment is attributed to the high-frequency impact of around 4000 Hz induced by the inconsistencies inherent in the manual method. Notably, several pads on both test boards had cables soldered to them, and these solder joints remained intact. The flexible cables likely absorbed most of the shock energy. The summarized test results are presented in Tables 6 and 7.

Table 6. Resistance Value Variations Resulting from Manual Pyroshock Tests (Sample #1).

Terminal	Pristine [mΩ]	After the Test [mΩ]	Change [mΩ]	Rate of Change [%]
T1	237.05	236.48	0.57	0.24
T3	329.95	328.13	1.82	0.55
T5	255.69	253.84	1.85	0.72

Table 7. Resistance Value Variations Resulting from Automated Pyroshock Tests (Sample #2).

Terminal	Pristine [mΩ]	After the Test [mΩ]	Change [mΩ]	Rate of Change [%]
T1	236.49	235.79	0.70	0.30
T3	334.23	333.77	0.46	0.14
T5	257.21	256.33	0.88	0.34

6. Conclusions

The similarity between the pyroshock tests and the analytical predictions were verified by the vibration wave analysis. By considering variables, including the pendulum weight, the pendulum angle, and the specimen installation position, the pyroshock analysis model effectively determined the necessary variables to meet given test requirements, thereby significantly reducing the trial-and-error process during actual tests. This pyroshock test prediction process enhanced the reliability and consistency of the test results. Additionally, by using the derived wave approach and the genetic algorithm, the process to satisfy the test requirements from approximately 2000 variable combinations was optimized. To address the issue of poor test repeatability, often affected by variations in pendulum angle, steel ball release method, and timing, the automated test equipment was designed and verified. Inspired by release assist devices, the automated test system incorporated a stopper to prevent rebound impact from the ball. This design ensured a consistent release process of the steel ball, minimized human error, and improved the repeatability of test results.

Comparison with the manual test methods demonstrated a significant improvement in the repeatability of the automated test method. The automated test method not only enhanced the accuracy and repeatability of the tests, but also reduced the workload and time required for each test. Tests were conducted on the same circuit boards using both manual and automated methods, confirming the impact of excessive high-frequency components.

Future research aims to further enhance the automated system by application of real-time feedback. Precision sensors and actuators may monitor and adjust the pendulum's motion, significantly improving accuracy and consistency. Various optimization techniques need to be explored to derive test conditions that meet test requirements. Through multiple trials, the developed automated test methods and condition predictions may be refined to identify and improve any shortcomings.

In conclusion, the accurate prediction of test conditions and the development of an automated testing system represent significant advancements in the field of pyroshock testing. Aerospace electronic components require considerable time for development and manufacturing. This research significantly contributes to preventing unnecessary delays and damage during the test process. These improvements, including the verification of the similarity between pyroshock tests and predictions, the effective determination and GA optimization of necessary test variables to meet test requirements, and the development of an automated test system capable of consistently implementing test conditions,

collectively enhance the reliability and repeatability of test procedures. Moreover, the automated test method not only improves accuracy and repeatability but also reduces the workload required for each test, thereby providing crucial benefits for mechanical durability validation of aerospace components.

Author Contributions: Conception and design, W.B. and J.P.; Data Collection, W.B.; Analysis and interpretation, W.B. and J.P.; Writing the article, W.B. and J.P. All authors have read and agreed to the published version of the manuscript.

Funding: This research was supported by the Korea Agency for Infrastructure Technology Advancement (KAIA) grant funded by the Ministry of Land, Infrastructure and Transport (RS-2022-0014-3396).

Data Availability Statement: The data presented in this study are available in article.

Conflicts of Interest: The authors declare no conflict of interest.

References

1. *ECSS-E-ST-10-03C*; Space Engineering—Testing. ECSS: Nice, France, 2022.
2. *NASA-STS-7003A*; Pyroshock Test Criteria. NASA: Washington, DC, USA, 2011.
3. *MIL-STD-810H*; Environmental Engineering considerations and Laboratory Tests. U.S. Department of Defense: Arlington, VA, USA, 2019.
4. *MIL-STD-1540D*; Product Verification Requirements for Launch, Upper-Stage, and Space Vehicles. U.S. Department of Defense: Arlington, VA, USA, 1999.
5. *ECSS-E-HB-32-25A*; Mechanical Shock Design and Verification Handbook. European Cooperation for Space Standardization: Noordwijk, The Netherlands, 2015.
6. Irvine, T. SRS Matlab Script (Kelly-Richman & Smallwood). Available online: https://www.vibrationdata.com/matlab.htm (accessed on 1 August 2023).
7. Sisemore, C. Shock Response Spectrum Primer. In Proceedings of the 91st Shock and Vibration Symposium, Orlando, FL, USA, 19–23 September 2021.
8. Lee, J.-R.; Chia, C.C.; Kong, C.-W. Review of Pyroshock Wave Measurement and Simulation for Space Systems. *Measurement* **2012**, *45*, 631–642. [CrossRef]
9. Irvine, T. An Introduction to the Shock Response Spectrum, Revision S; 2012. Available online: https://www.vibrationdata.com/tutorials2/srs_intr.pdf (accessed on 1 March 2023).
10. Davie, N.T.; Bateman, V.I. Pyroshock testing, chapter 26, part 2. In *Harris' Shock and Vibration Handbook*; Sandia National Laboratories: Albuquerque, NM, USA, 1996.
11. Davie, N.T.; Bateman, V.I. Pyroshock Simulation for Satellite Components Using a Tunable Resonant Fixture-Phase 1; SAND 92-2135; 1992. Available online: https://www.osti.gov/biblio/6897405 (accessed on 15 July 2022).
12. Davie, N.T. Simulation of Pyroshock Environments Using a Tunable Resonant Fixture. U.S. Patent 5,565,626, 15 October 1993.
13. Kolaini, A.R.; Nayeri, R.; Kerm, D.L. Pyroshock Simulation Systems: Are We Correctly Qualifying Flight Hardware for Pyroshock Environments? In Proceedings of the 25th Aerospace Testing Seminar, Pasadena, CA, USA, 12–15 October 2009.
14. Ding, J.; Sun, Y.; Dang, Y. Pyroshock Response Prediction of Spacecraft Structure in Wide Frequency Domain Based on Acceleration FRF. *Aerospace* **2022**, *9*, 54. [CrossRef]
15. Choi, M. Experimental Prediction of Shock Response Spectra of Point-Wise Explosive Pyroshock in a Space Launcher Composite Structure Using Laser Pulse Excitation and In-line Filtering. *SAE Int. J. Aerosp.* **2013**, *6*, 65–69. [CrossRef]
16. Wang, X.; Yu, T.; Yan, H.; Ding, J.; Li, Z.; Qin, Z. Application of Stress Wave Theory for Pyroshock Isolation at Spacecraft-Rocket Interface. *Initiat. Pyrotech.* **2007**, *5*, 5–8. [CrossRef]
17. Yalçinkaya, T.; Gürsoy, B. Numerical Validation of a Pyroshock Test System and Application to Qualification Tests. *Aerospace* **2022**, *9*, 400. [CrossRef]
18. Gour, S.; Ahmad, D.; Kumar, D.; Ajaj, R.M.; Zweiri, Y. Investigating the Tear Fracture of Elastomeric Skins in Morphing Wings: An Experimental and Computational Study. *Int. J. Appl. Mech.* **2023**, *15*, 2350096. [CrossRef]
19. Sun, W.; Su, Q.; Yuan, H.; Chen, S. Performance Analysis of Absolute Acceleration Shock Response Spectrum. *J. Phys. Conf. Ser.* **2020**, *1676*, 012131. [CrossRef]
20. Sun, W.; Su, Q.; Yuan, H.; Liu, L. Calculation and Characteristic Analysis on Different Types of Shock Response Spectrum. *J. Phys. Conf. Ser.* **2020**, *1676*, 012236. [CrossRef]
21. Tuma, J.; Koci, P. Calculation of a Shock Response Spectrum. In Proceedings of the International Carpathian Control Conference (ICCC), Prague, Czech Republic, 3–4 February 2011.
22. Almesmari, A.; Jarrar, F.; Almaskari, F.; Marpu, P.R.; Abdul Shukoor, N.; Govindan, J.K. Development of a Metal-to-Metal Mid-Field Shock Test Procedure for Nanosatellites. *IEEE J. Miniaturization Air Space Syst.* **2020**, *1*, 103–109. [CrossRef]
23. Kiryenko, S.; Piret, G.; Kasper, J. *ESA ESTEC Shock Bench Presentation*; European Space Agency: Paris, France, 2005.

24. Binder, J.; McCarty, M.; Rasmussen, C. *Development of a Pyrotechnic Shock Simulation Apparatus for Spacecraft Applications*; California Polytechnic State University: San Luis Obispo, CA, USA, 2012.
25. Lacher, A.; Jüngel, N.; von Wagner, U.; Bäcker, A. Analytical Calculation of In-Plane Response of Plates with Concentrated Masses to Impact and Application to Pyroshock Simulation. *J. Sound Vib.* **2012**, *331*, 3358–3370. [CrossRef]
26. Smith, J.; Brown, A. Analysis of the Shock Response Spectrum and Resonant Plate Testing Methods. *J. Aerosp. Test.* **2019**, *45*, 631–645.
27. Jung, J.R.; Kim, I.G.; Lee, S.J.; Kang, C.H. Characteristics of the shock response spectrum for structures subjected to pyroshock. In Proceedings of the Korean Society for Aeronautical & Space Sciences Spring Conference, Gyeongju, Republic of Korea, 13–15 April 2011.
28. Jeon, H.; Kim, M.; Kim, M.; Kwon, Y.; Yu, Y.; Kim, I. The Parametric Study of the Design Variables on the SRS of Pyroshock Resonant Bar. *J. Korea Inst. Mil. Sci. Technol.* **2018**, *21*, 413–421.
29. Jonsson, M. Development of a Shock Test Facility for Qualification of Space Equipment. Master's Thesis, Chalmers University of Technology, Department of Applied Mechanics, Division of Dynamics, Göteborg, Sweden, 2012; pp. 1–96.
30. Charvet, B.; Dilhan, D.; Palladino, M. Shock Bench Enhancements. In Proceedings of the 13th European Conference on Spacecraft Structures, Materials & Environmental Testing, Braunschweig, Germany, 1–4 April 2014.
31. Küçükbayram, A.İ. Analysis and Verification of a Pyroshock Test System. Master's Thesis, Department of Mechanical Engineering, Middle East Technical University, Ankara, Turkey, 2021; pp. 1–12.
32. Adebolu, I.O.; Masui, H.; Cho, M. Quantitative Evaluation of SRS Similarity for Aerospace Testing Applications. *J. Aerosp. Test.* **2021**, *29*, 123–136. [CrossRef]
33. Davie, N.T.; Bateman, V.I. Recent Developments in Pyroshock Simulation Using Fixtures with Tunable Resonant Frequencies. *Proc. Inst. Environ. Sci.* **2020**, *46*, 77–89.
34. Zhang, L.; Wang, J. Research on Impact Reduction of Flexible Boundary Particle Damping Honeycomb Plate Based on Discrete Element Multi-Body Dynamics Coupling. *J. Aerosp. Eng.* **2019**, *32*, 405–418.
35. Kolaini, A.R.; Fernandez, J.P. JPL Tunable Beam Pyroshock Simulation System. In Proceedings of the Spacecraft & Launch Vehicle Dynamic Environments Workshop, El Segundo, CA, USA, 26–28 June 2007; pp. 1–12.
36. Lee, S.-J.; Hwang, D.-H.; Han, J.-H. Development of Pyroshock Simulator for Shock Propagation Test. *Shock. Vib.* **2018**, 9753793. [CrossRef]
37. Garnier, J.; De Fruytier, C. Experimental Shock Damage Risk Assessment for New Generation TAS-B Plasmic Propulsion Unit. In Proceedings of the 13th European Conference on Spacecraft Structures, Materials & Environmental Testing, Braunschweig, Germany, 1–4 April 2014.
38. Spletzer, M.; Sisemore, C. Design of a Resonant Plate Shock Fixture to Attenuate Excessive High-Frequency Energy Inputs. In Proceedings of the 87th Shock and Vibration Symposium, New Orleans, LA, USA, 17–20 October 2016.
39. Titulaer, J.J.; Allen, B.R.; Maly, J.R. *An Alternative to Pyrotechnic Testing for Shock Identification*; CSA Engineering, Inc.: Mountain View, CA, USA, 2008.
40. Gambler, F.; Conti, C.; Dehombreux, P.; Filippi, E. Development of a Test Facility to Simulate Pyroshock Environments in a Laboratory. *Trans. Built Environ.* **1998**, *32*, 274–282.
41. Hwang, D.-H.; Park, H.-S.; Han, J.-H. Development of a Miniature Point Source Pyroshock Simulator. *J. Sound Vib.* **2020**, *481*, 115438. [CrossRef]
42. Jeong, J.-W.; Lim, J.-H.; Kim, K.-W.; Lee, J.-J. Development of a Point Pyroshock Source Simulator. *Shock. Vib.* **2017**. [CrossRef]
43. Kim, B.-S.; Lee, J. Development of Impact Test Device for Pyroshock Simulation Using Impact Analysis. *Aerospace* **2022**, *9*, 407. [CrossRef]
44. Adebolu, I.O. Evaluation of Shock Response Spectrum Similarity and Repeatability in the Qualification Testing of Space Components. Ph.D. Thesis, Kyushu Institute of Technology, Fukuoka, Japan, 2021.
45. RAL Space. First Pyroshock Tests Completed at RAL Space. RAL Space. 2020. Available online: https://www.ralspace.stfc.ac.uk/Pages/First-pyroshock-tests-completed-at-RAL-Space.aspx (accessed on 3 May 2024).
46. MTES Pyroshock Test. MTES. Available online: http://mtes.co.kr/sub/sub2_2_2.php (accessed on 3 May 2024).
47. Beyond Gravity Switzerland Pyroshock Test. Available online: https://triasrnd.com/l/93-pyroshock-test (accessed on 3 May 2024).
48. DLR—Institute of Space Systems. Mechanical-Dynamical Test Facilities: Pyroshock. Laboratories Brochure. Available online: https://www.dlr.de/en/irs/media/publications/institute-brochures (accessed on 3 May 2024).
49. Astrofein. Environmental Simulation. Astrofein. Available online: https://www.astrofein.com/en/environmental-simulation/ (accessed on 3 May 2024).
50. von Wagner, U.; Jüngel, N.; Ritzmann, S.; Bäger, A. Simulation of Pyroshocks. In Proceedings of the 1st CEAS European Air and Space Conference, Berlin, Germany, 10–13 September 2007.
51. Goldberg, D.E. *Genetic Algorithms in Search, Optimization, and Machine Learning*; Addison-Wesley: Boston, MA, USA, 1989.
52. Gen, M.; Cheng, R. *Genetic Algorithms and Engineering Design*; John Wiley & Sons: Hoboken, NJ, USA, 1997.
53. Sun, W.; Huang, Y.; Chen, H. An Improved Adaptive Genetic Algorithm for Optimizing Pyroshock Acceleration Synthesis. *IEEE Access* **2019**, *7*, 132682–132692. [CrossRef]

54. Viale, L.; Daga, A.P.; Garibaldi, L. Design of a Resonant Plate for Pyroshock Testing Based on Shape and Size Heuristic Optimization. 2023. Available online: https://hal.science/hal-04179596/document (accessed on 1 May 2024).
55. Viale, L.; Daga, A.P.; Fasana, A.; Garibaldi, L. On pyroshock tests for aerospace equipment qualification: A comprehensive parametric model for the simulation and the design of pyroshock test facilities. *Int. J. Impact Eng.* **2023**, *180*, 104697. [CrossRef]
56. Monti, R.; Gasbarri, P. Dynamic load synthesis for shock numerical simulation in space structure design. *Acta Astronaut.* **2017**, *137*, 222–231. [CrossRef]
57. Chen, J.; Jiang, J.; Wang, K.; Zhang, F. Optimal Placement of Actuators for Active Vibration Control Using EER and Genetic Algorithm. In Proceedings of the 2019 IEEE 10th International Conference on Mechanical and Aerospace Engineering (ICMAE), Brussels, Belgium, 22–25 July 2019; pp. 449–453.
58. Brüggemann, T.; Biermann, D.; Zabel, A. Development of an Automatic Modal Pendulum for the Measurement of Frequency Responses for the Calculation of Stability Charts. *Procedia CIRP* **2015**, *33*, 587–592. [CrossRef]

Disclaimer/Publisher's Note: The statements, opinions and data contained in all publications are solely those of the individual author(s) and contributor(s) and not of MDPI and/or the editor(s). MDPI and/or the editor(s) disclaim responsibility for any injury to people or property resulting from any ideas, methods, instructions or products referred to in the content.